Science Advances
AAAS

Supplementary Materials for

A beneficial environment promotes immune resilience through epigenetic regulation

Guilherme Dragunas *et al.*

Corresponding author: Ali Önder Yildirim, oender.yildirim@helmholtz-munich.de

Sci. Adv. **12**, eady7317 (2026)
DOI: 10.1126/sciadv.ady7317

This PDF file includes:

Figs. S1 to S10

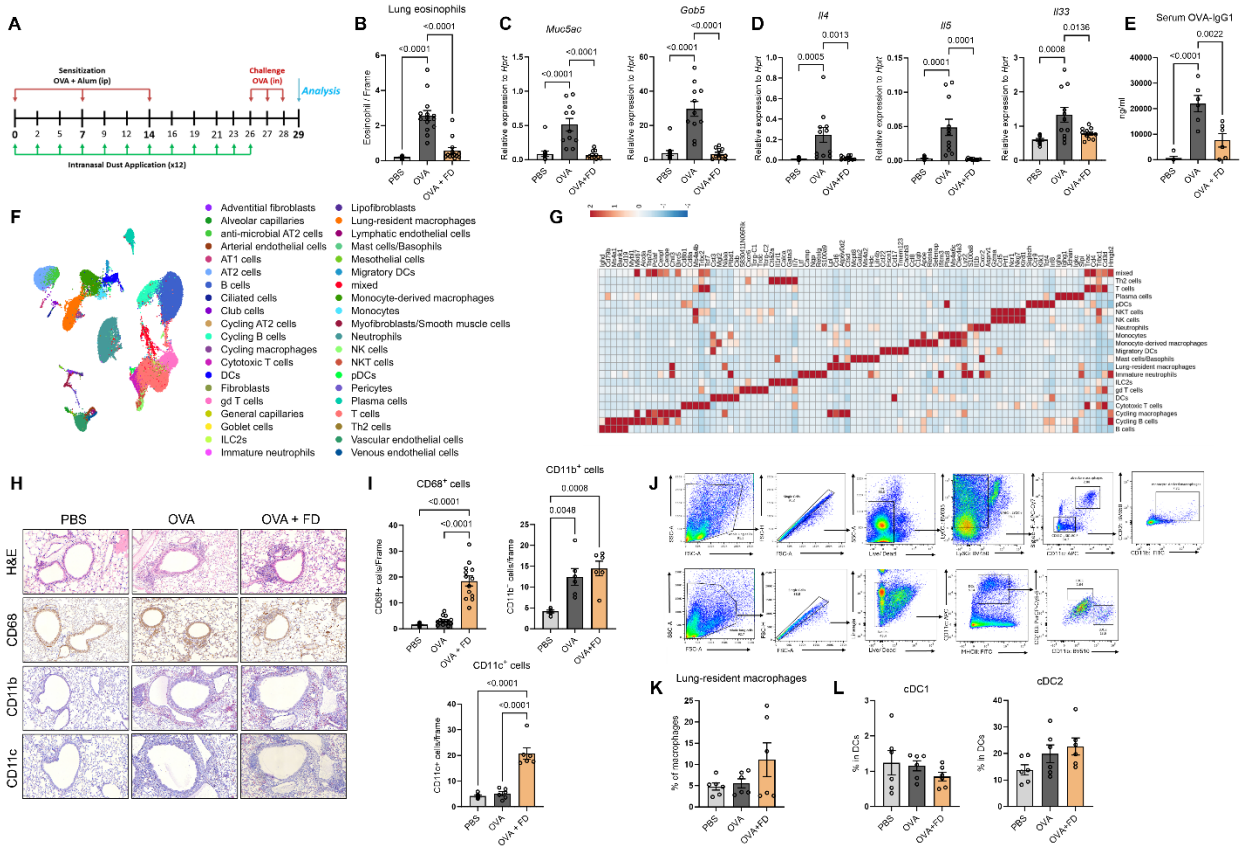

Figure S1. Preventive exposure to FD reduces airway inflammation and changes the profile of lung infiltrating immune cells. (A) Experimental protocol used. (B) RT-qPCR analysis from whole lung homogenates detecting the expression of type-2 immune cytokines *Il4*, *Il5* and *Il33* genes. (C) Quantification of airway eosinophils from lung sections. (D) RT-qPCR analysis from whole lung homogenates detecting the expression of mucus associated *Muc5ac*, *Gob5* and *Spdef* genes. (E) Serum titers of anti-OVA specific IgG1. (F) UMAP plot from all cell types annotated from the whole lung homogenates submitd to scRNAseq. (G) Markers used to annotate immune cells and heatmap map from pseudobulk counts of marker genes for each cell type. (H) Representative airway histological sections stained with H&E and immunostained for CD68, CD11b and CD11c and (I) quantified for the presence of $CD68^{+}$, $CD11b^{+}$ and $CD11c^{+}$ cells. (J) Gating strategy employed to discriminate $CD45^{+}$, $Ly6g^{neg}$, $F4/80^{+}$, $CD11c^{neg}$, $F4/80^{+}$, $CCR2^{+}$, $SiglecF^{neg}$ monocyte-derived macrophages, $CD45^{+}$, $Ly6g^{neg}$, $F4/80^{+}$, $CD11c^{+}$, $CD11b^{neg}$, $CCR2^{neg}$, $SiglecF^{+}$ lung-resident macrophages, $CD45^{+}$, $CD11c^{+}$, $MHCII^{+}$ dendritic cells (DCs), subdivided into $CD11^{bneg}$, $CD103^{+}$ cDCs1, $CD11b^{+}$, $CD103^{neg}$, $CD64^{neg}$ cDC2 and $CD11b^{+}$, $CD103^{neg}$, $CD64^{+}$ monocyte-derived cDCs. (K) Frequency of lung-resident macrophages within parent gate compared between conditions. (L) Frequency of cDC1 and cDC2 within parent gate compared between conditions. Results are plotted as mean ±SEM and difference between means were compared using One-way ANOVA followed by Tukey post-hoc test (n=6-9).

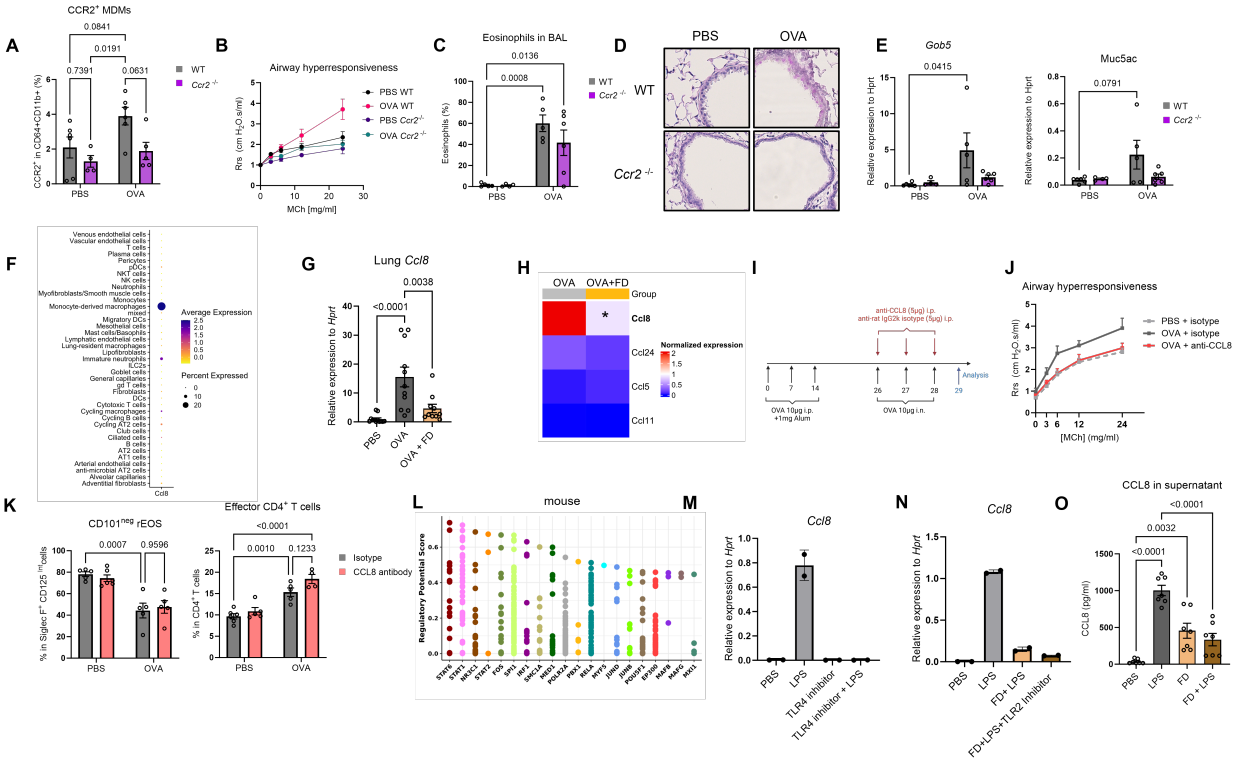

Figure S2. *Ccr2*$^{-/-}$ mice display reduced allergic airway inflammation to OVA, while MDMs from OVA+FD express reduced M2 related markers. (A) *Ccr2*$^{-/-}$ and WT C57BL/6 mice were submitted to the same OVA induced allergic airway inflammation protocol, as described. The percentage of lung CCR2^{+} MDMs was quantified in relation to CD64^{+} CD11b^{+} cells. (B) Airway resistance measured after increasing concentrations of nebulized methacholine to anesthetized mice. (C) BAL eosinophilia quantified in stained slides. (D) Representative images from PAS-stained lung airways. (E) RT-qPCR analysis of the mucus-related genes *Gob5* and *Muc5ac* in total lung homogenates. (F) *Ccl8* average gene expression within each annotated immune cell type. (G) The gene expression of *Ccl8* was assessed in whole lung homogenates using RT-qPCR. (H) Normalized gene expression from *Ccl8*, *Ccl24*, *Ccl5* and *Ccl11* within MDMs, comparing OVA and OVA+FD groups. (I) Experimental protocol used for blocking CCL8 signalling via administering sensitized mice anti-CCL8 antibody before OVA intranasal challenges. (J) Airway resistance measured after increasing concentrations of nebulized methacholine to anesthetized mice receiving anti-CCL8 antibody or isotype control. (K) Quantification of CD45^{+}, Ly6g^{neg}, CD125^{int}, SiglecF^{+}, CD11c^{+}, CD101^{neg} resident eosinophils and CD45^{+}, CD4^{+}, CD62L^{neg}, CD44^{+} effector T cells within the whole lung homogenates of mice receiving anti-CCL8 via FACS. (L) CistromeDB Toolkit was used to assess potential transcription factor binding within 10kb from gene TSS in mouse mm10 genome.

(M) *Ccl8* gene expression regulation in response to LPS stimulation was assessed via RT-qPCR. 1h before LPS was added to the cells, resatorvid (Res, TLR4 inhibitor) was preventively given.

(N) BMDMs were pretreated with the TLR2 inhibitor C29 (1 h) before stimulation with FD for 24 h, followed by an additional 24 h of FD exposure. *Ccl8* gene expression was assessed via RT-qPCR (O) CCL8 protein levels were measured by ELISA in supernatant from LPS stimulated hPBMC-derived monocytes and pre-treated with 48h of FD. Results are plotted as mean ±SEM and difference between means were compared using One-way ANOVA or Two-way ANOVA, where appropriate, followed by Tukey post-hoc test (n=2-6).

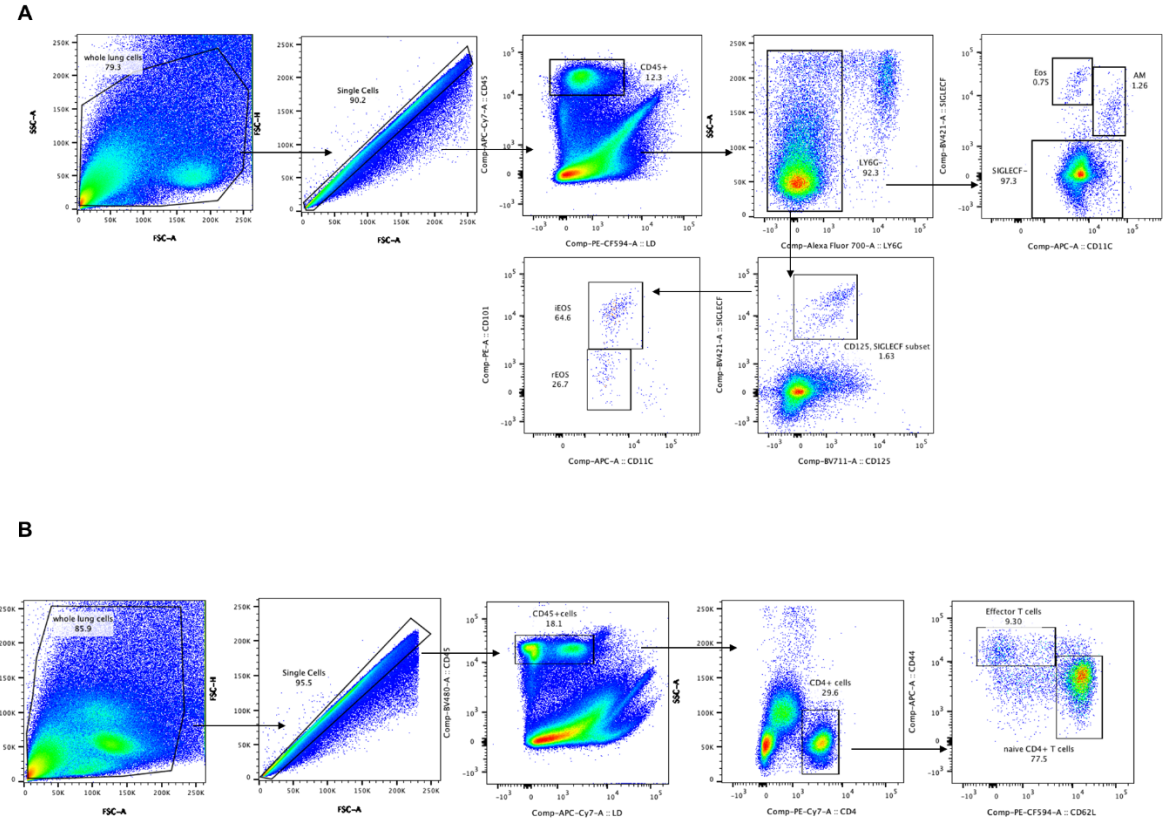

Figure S3. Gating strategy employed to discriminate (A) $CD45^{+}$, $Ly6g^{neg}$, $CD125^{int}$, $SiglecF^{+}$, $CD11c^{+}$, $CD101^{+}$ recruited inflammatory eosinophils and $CD45^{+}$, $Ly6g^{neg}$, $CD125^{int}$, $SiglecF^{+}$, $CD11c^{+}$, $CD101^{neg}$ resident eosinophils and (B) $CD45^{+}$, $CD4^{+}$, $CD44^{+}$, $CD62L^{neg}$ effector T cells in whole lung homogenates from anti-CCL8 antibody treated mice.

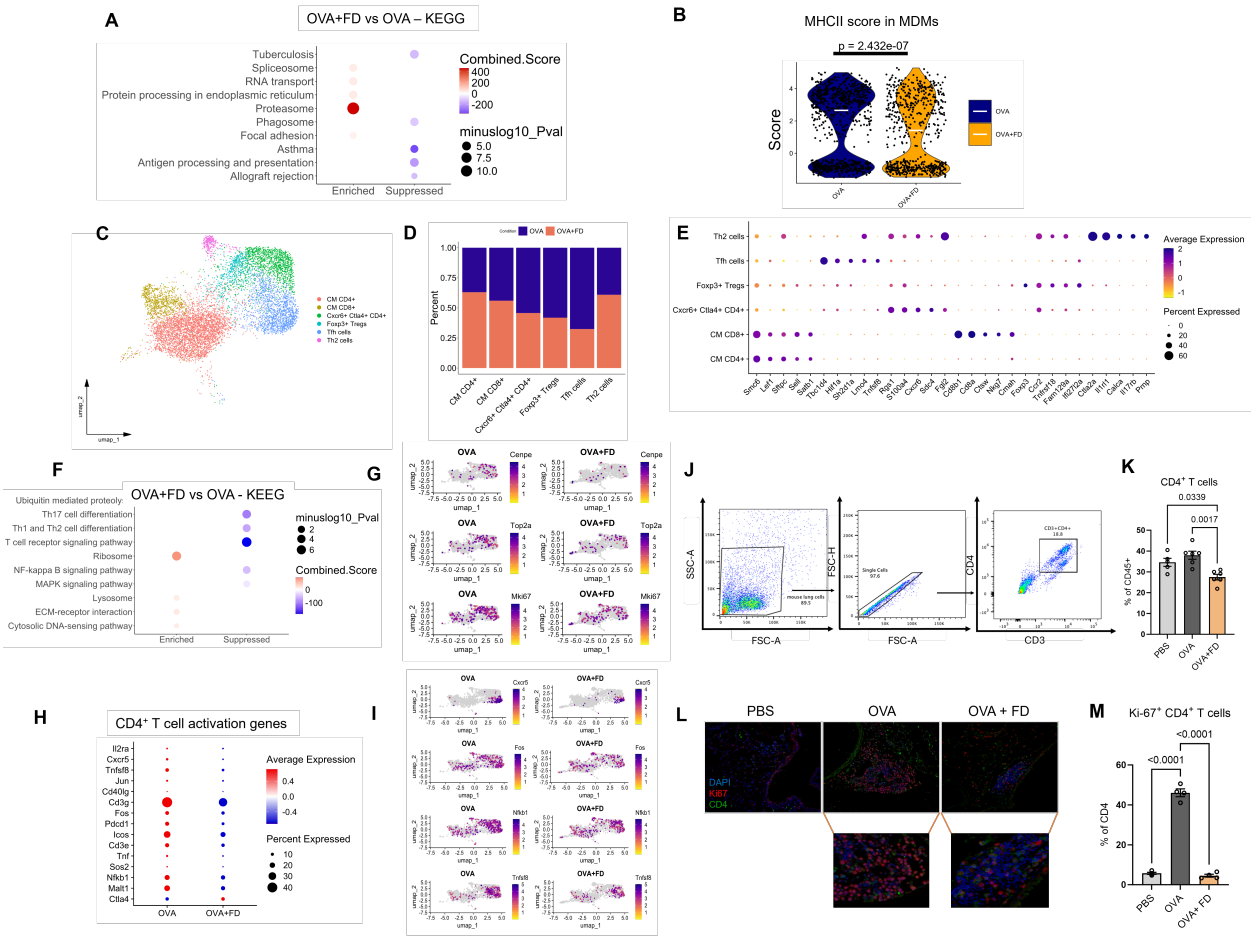

Figure S4. CD4⁺ T cell lung composition and the expression of T cell activation and proliferation related genes are reduced in OVA+FD group compared to OVA as a result of reduced MHCII expression. (A) A list of KEGG pathways enriched and supressed comparing OVA and OVA+FD MDMs was generated using *EnrichR* package in lung scRNAseq data. (B) A list of MHCII related genes (Reactome R-MMU-2132295) was used to assign a socre to each MDM subset cell in scRNAseq analysis using *AddModuleScore* function. Later, the score was compared between OVA and OVA+FD groups and statistical significance between means was assessed via Student´s T-test. (C) T cells were subset and plotted in an UMAP space to highlight differences between gene expression composition within the lungs of OVA and OVA+FD groups. Clusters were generated using classical Leuvian clustering and highlighted with different colours and numbers before embedding into the UMAP plot. (D) The frequency of each T cell cluster comparing OVA+FD and OVA groups (E) Top expressed genes used for clustering. (F) OVA+FD and OVA cells were compared using gene set enrichment analysis and the KEGG database applied to define enriched and suppressed pathways in OVA+FD group. (G) Proliferation genes *Mki67*, *Top2a* expression were plotted within UMAP space, comparing OVA and OVA+FD groups. (H) Average expression from genes associated with T cell activation and inflammation were plotted (I) The genes associated with T cell activation *Cxcr5*, *Fos*, *Nfkb1* and *Tnfsf8* were plotted within UMAP space, comparing OVA and OVA+FD groups. (J) Whole lung homogenates were submitted to FACS analysis. Gating strategy to discriminate CD3⁺, CD4⁺ T cells is shown. (K) Quantification of CD4⁺ T cells within the lungs. (L) Representative immunofluorescence staining of lung sections from mice and the (M) quantification of double positive CD4/Ki67 cells. Results are plotted as mean ±SEM and difference between means were compared using One-way ANOVA followed by Tukey post-hoc test (n=4-6).

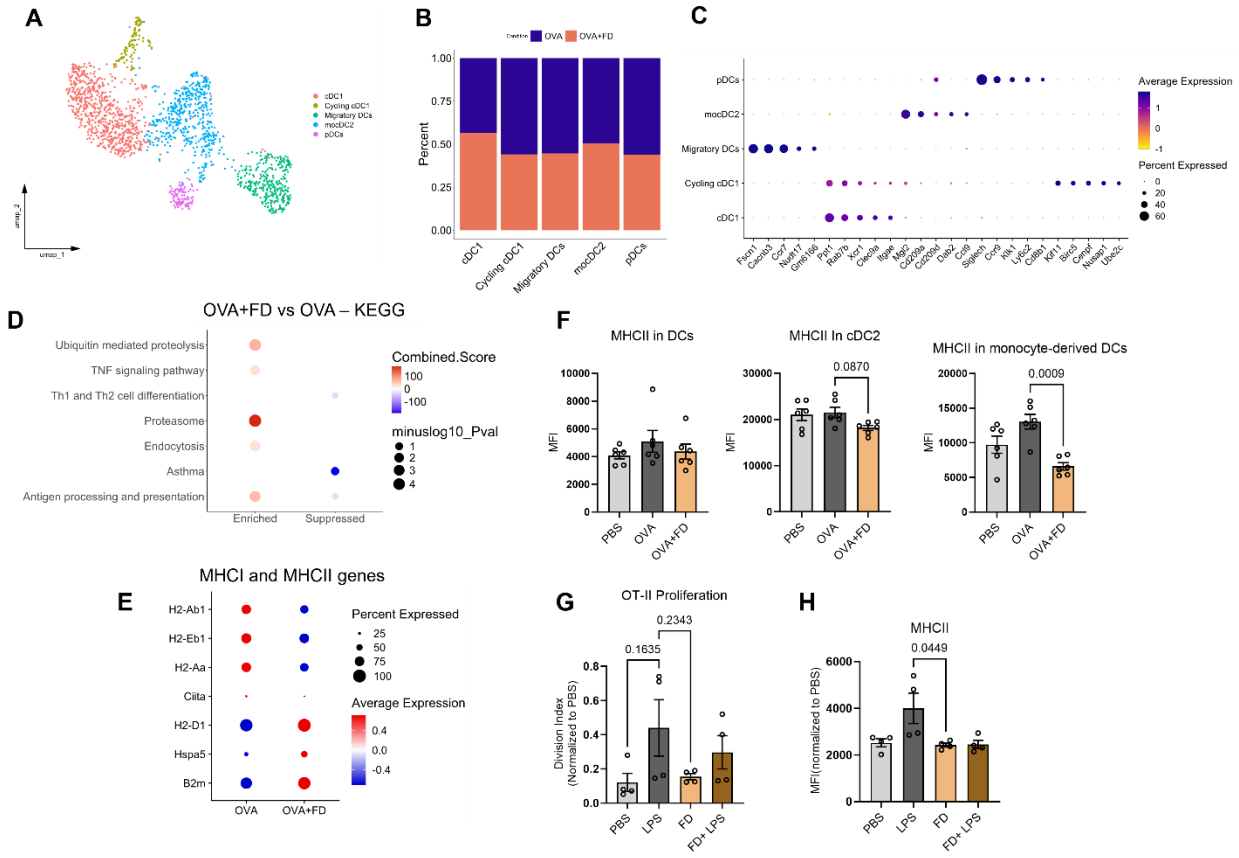

Figure S5. Dendritic cell lung composition and the expression of MHCII genes are reduced, while the expression of MHCI genes are increased in OVA+FD group compared to OVA. (A) DCs were subset and plotted in an UMAP space to highlight differences between gene expression composition within the lungs of OVA and OVA+FD groups. Clusters were generated using classical Leuvian clustering at resolution 0.3 and highlighted with different colours and number before embedding into the UMAP plot. (B) The frequency of each DC cluster comparing OVA+FD and OVA groups. (C) Top expressed genes used for clustering. (D) OVA+FD and OVA DCs were compared using gene set enrichment analysis and the KEGG database applied to define enriched and suppressed pathways in OVA+FD group. (E) Leading edge genes from Antigen Processing and Presentation pathway are plotted, comparing expression levels of MHC-II and MHC-I genes in migratory DCs. (F) Whole lung homogenates submitted to flow cytometry are gated for total DCs, cDC2 and monocyte-derived DCs and MFI from expression levels of MHCII are plotted. (G) BMDCs were differentiated and stimulated during 48h with FD extract, followed by 6h of LPS and pulsed with $OVA_{323-339}$ peptide. Next, they were co-cultured with naïve $CD44^{neg}$, $CD62L^{+}$, $CD3^{+}$, $CD4^{+}$ T cells, which were stained with proliferation marker CTV. Afterwards, flow cytometry was performed to evaluated CTV-MFI derived division index. (H) MHCII membrane MFI was measured via flow cytometry in BMDCs that were exposed to FD and 1ng/ml or 10ng/ml LPS. Results are plotted as mean ±SEM and difference between means were compared using One-way ANOVA followed by Tukey post-hoc test (n=4-6).

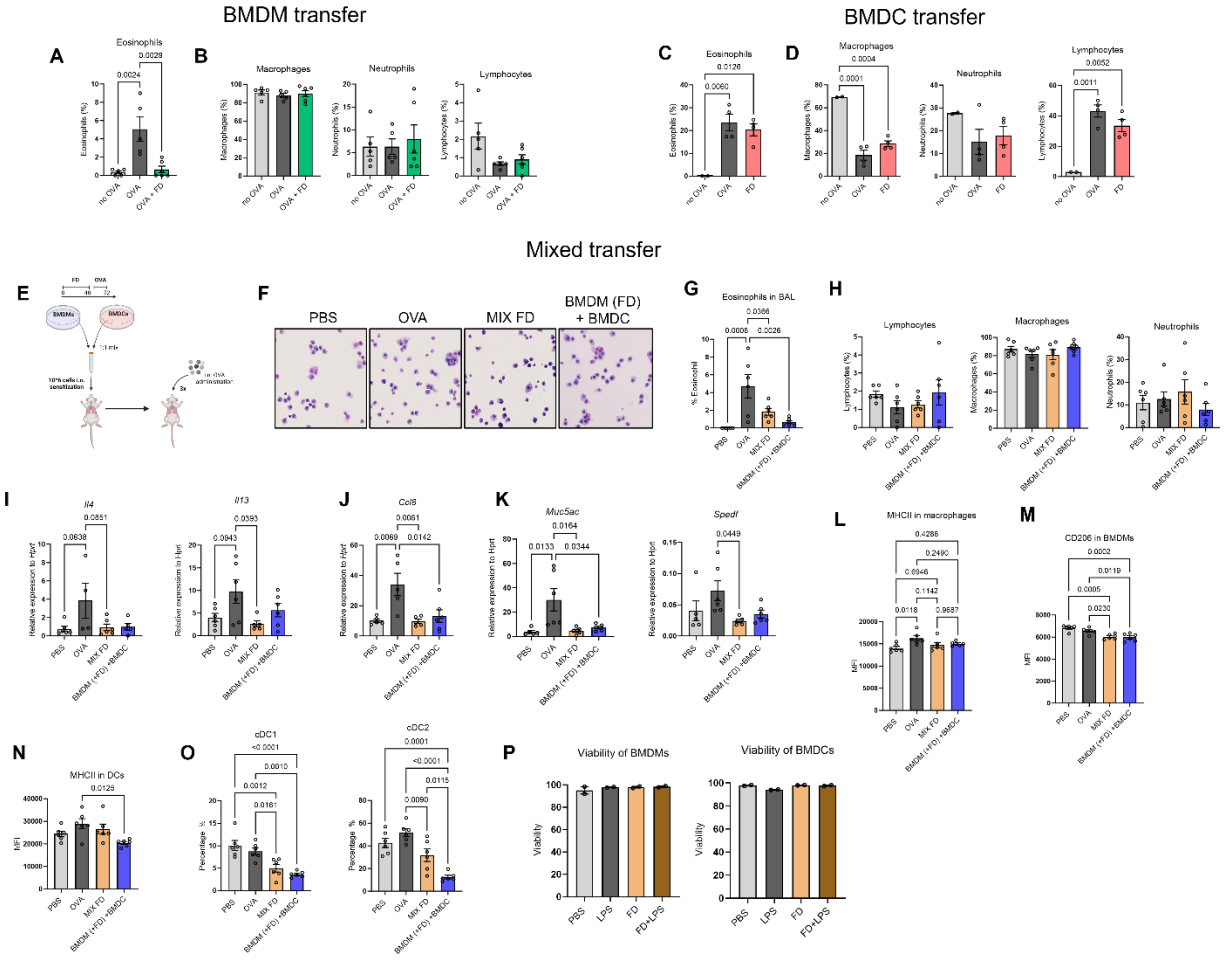

Figure S6. Intratracheal transfer of mixed BMDMs and BMDCs identifies a crucial role for BMDMs in modulating FD preventive effects on allergen sensitization. BMDMs and BMDCs were treated during 48h with FD, followed by overnight pulsing with OVA and intratracheal transfer to naïve Balb/c mice. 7 days later, the animals received three daily challenges with intranasal OVA. A-B: BMDM transfer. (A) Frequency of recovered BAL eosinophils (B) Frequency of macrophages, neutrophils, and lymphocytes in differential counted BAL. C-D = BMDC transfer: (C) Frequency of recovered BAL eosinophils. (D) Frequency of macrophages, neutrophils, and lymphocytes in differential counted BAL. E-O = mixed transfer: BMDMs and BMDCs were stimulated during 48h with FD extract, followed by pulsing with OVA overnight. In MIX FD group, both BMDMs and BMDCs were exposed to FD, whereas in BMDM(FD)+BMDC group, only the first cell type (BMDMs) was exposed to FD. Next, BMDMs and BMDCs were mixed at a 1:1 proportion and 10^6 cells were intratracheally delivered to naïve Balb/c mice. After 7 days, mice were challenged three times daily intranasally with OVA to induce airway allergic inflammation. (E) Graphical abstract depicting the protocol used. (F) Representative pictures from BAL cells recovered from each group. (G) Frequency of recovered BAL eosinophils. (H) Frequency of macrophages, neutrophils, and lymphocytes in differential counted BAL. (I) Th2-related cytokines gene expression *Il4* and *Il13* were assessed in lung homogenates via RT-qPCR. (J) *Ccl8* gene expression was assessed in lung homogenates via RT-qPCR. (K) Mucus-associated genes *Muc5ac* and *Spedf* were measured in lung homogenates via RT-qPCR. (L) MHCII surface expression in macrophages from lung homogenates. (M) Surface expression of M2 polarization marker CD206 on MDMs within the lungs. (N) MHCII surface expression in DCs from lung homogenates. (O) Frequencies of $CD103^+$ cDC1s and $CD11b^+$ cDC2s within total DC population in lung homogenates. (P) Viability of BMDMs and BMDCs. Prior to transfer, BMDMs and BMDCs were assessed for viability using a FACS-based live/dead dye staining assay. Both BMDMs and BMDCs exhibited high viability. Results are shown as mean ±SEM and difference between means were compared using One-way ANOVA followed by Tukey post-hoc test (n=2-6).

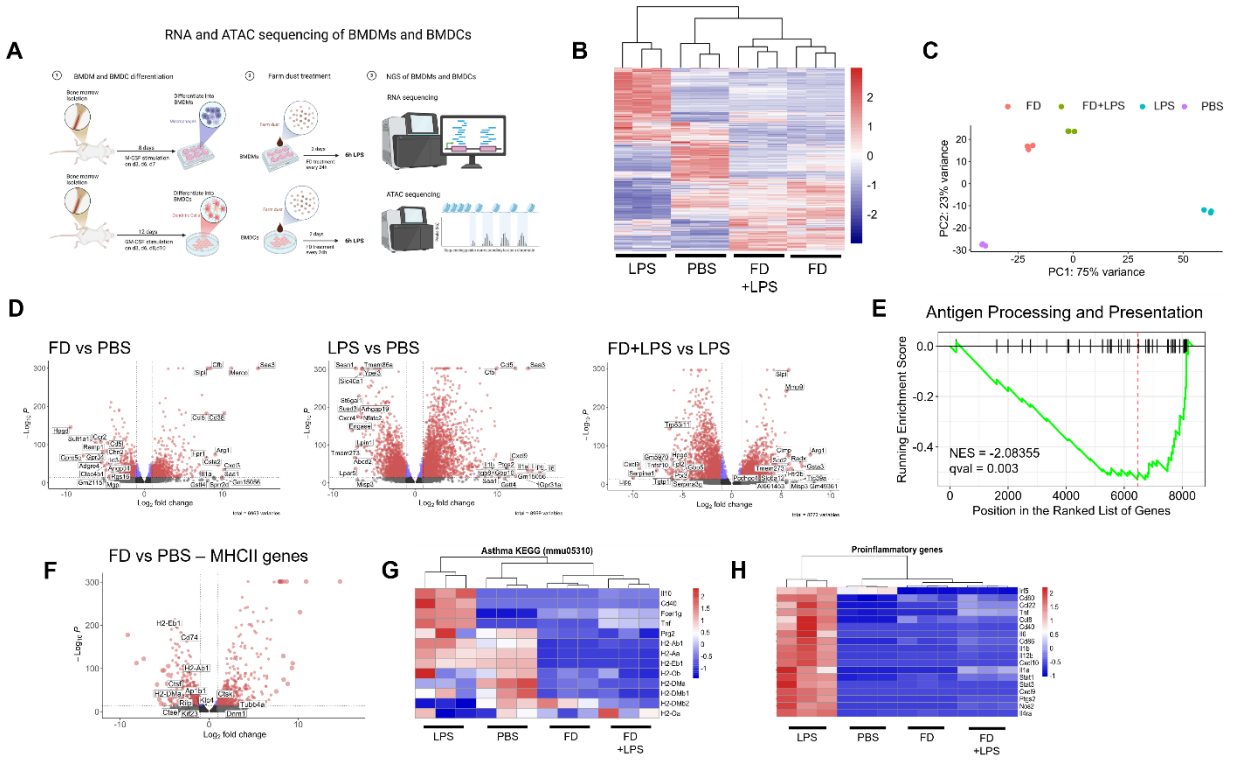

Figure S7. Bulk RNA-seq data from FD exposed BMDMs shows dampening of MHC-II related presentation and asthma associated genes. (A) Graphical abstract depicting the protocol used for BMDM and BMDC isolation, differentiation, and exposure to treatment conditions, which were later submitted to RNA-seq and ATAC-seq analysis. (B) Unbiased heatmap of z-normalized gene expression highlighting different gene expression patterns across experimental groups. (C) 2D-PCA plot highlighting transcriptional differences between treatment conditions. (D) Volcano plot for pairwise comparisons between experimental groups highlighting differently expressed genes (DEGs). (E) Gene set enrichment analysis (GSEA) highlighting suppression in KEGG pathway Antigen Processing and Presentation (mmu04612) in FD exposed BMDMs. (F) Volcano plot highlighting MHC-II associated genes from KEGG pathway Antigen Processing and Presentation (mmu04612) mainly downregulated, when comparing FD vs PBS groups. (G) Heatmap from z-normalized expression from genes belonging to Asthma (mmu05310) KEGG pathway. (H) Heatmap from z-normalized expression from genes belonging to pro-inflammatory genes.

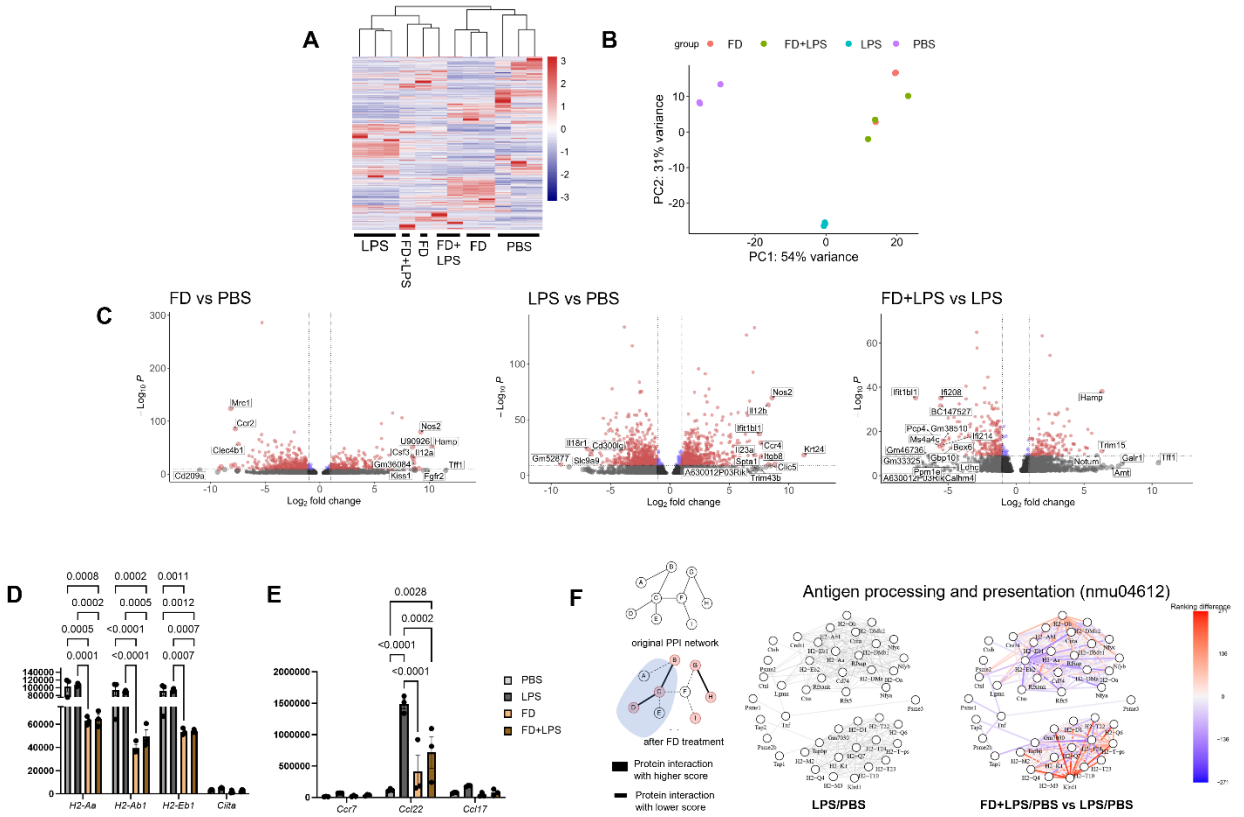

Figure S8. RNA-seq from BMDCs exposed to FD demonstrate dampened MHCII gene expression and decreased expression of lymph node migration and Th2 polarization related genes. (A) Unbiased heatmap of z-normalized gene expression highlighting different gene expression patterns across experimental groups. (B) 2D-PCA plot highlighting transcriptional differences between treatment conditions. (C) Volcano plot from pairwise comparisons between experimental groups highlighting DEGs. (D) Normalized counts from MHCII related genes *H2-Aa*, *H2-Ab1*, *H2-Eb1* and *Ciita*. (E) Normalized counts from lymph node migration and Th2 polarization genes *Ccr7*, *Ccl22* and *Ccl17.* (F) BMDCs were stimulated for 48h with FD extract, followed by 6h of LPS. Afterwards, RNA was isolated and submitted to bulk sequencing. High confidence curated protein-protein interaction (PPIs) (human-mouse orthologs) network was generated from published datasets. Next, KEGG and Reactome pathways were used to generate functional modules and PPI scores were calculated inside such modules, taking into consideration the magnitude of changes in gene expression levels and the directional relationship of the expression profiles across two conditions. Antigen processing and presentation module network is shown, containing straightened and weakened PPIs comparing BMDCs bulk RNAseq data of LPS vs FD+LPS groups, using PBS as groups as baseline. Results are shown as mean ±SEM and difference between means were compared using One-way ANOVA followed by Tukey post-hoc test (n=3-4).

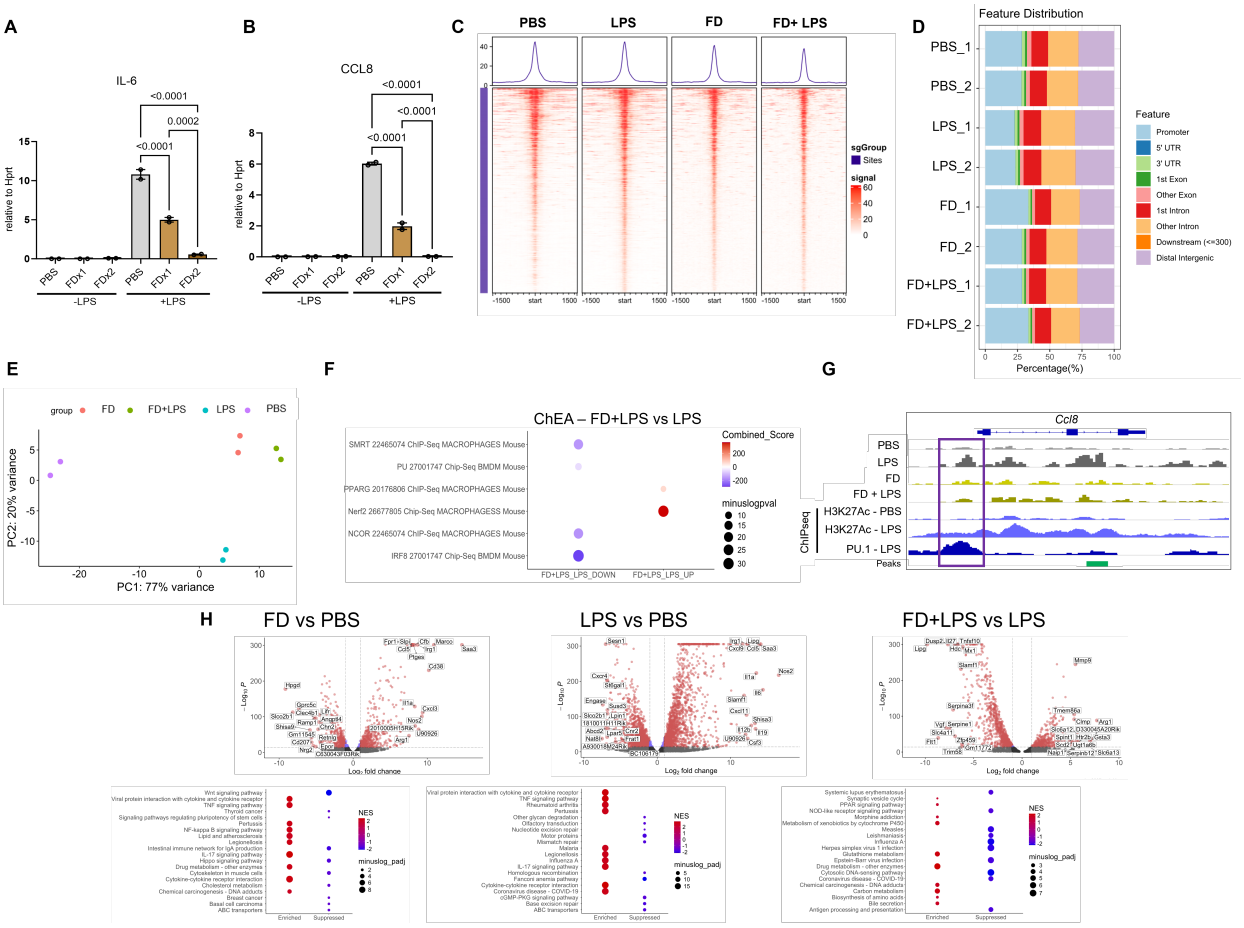

.

Figure S9. ATAC-seq of BMDCs exposed to FD and LPS. (A) THP1 cells, differentiated into macrophage-like cells using PMA (24 h), were treated with FD either once or twice. Repeated FD treatment consistently produced a stronger modulatory effect compared to a single application. Results are plotted as mean ±SEM and difference between means were compared using One-way ANOVA (n=2). (B) Merged peak regions annotated are shown as an accessibility heatmap. (C) Gene regions of annotated peaks across experimental groups. (D) 2D-PCA plot from DESeq2 normalized OCRs across experimental conditions. (E) Differential number of OCRs analysed via DESeq2. (F) HOMER motif analysis of transcription factors enriched in UP (open chromatin in FD) and DOWN (open chromatin in PBS) peaks. (G) IGV tracks of ATAC-seq BigWig files from each experimental replicate and ChIPseq data from p65 and H3K27Ac in LPS exposed BMDCs, overlayed into mm10 genome. *Ciita* and *H2-Eb1* genes are shown. (H) BMDCs were submitted to ATAC-seq for chromatin accessibility analysis and differential open chromatin regions (OCRs) after pairwise comparison between groups using DESeq2 were integrated with significantly up- or downregulated genes in bulk RNA-seq analysis. A linear regression was traced using z-scaled log2FC from RNA-seq DEGs and ATAC-seq significant ($p<0.05$) differential OCRs.

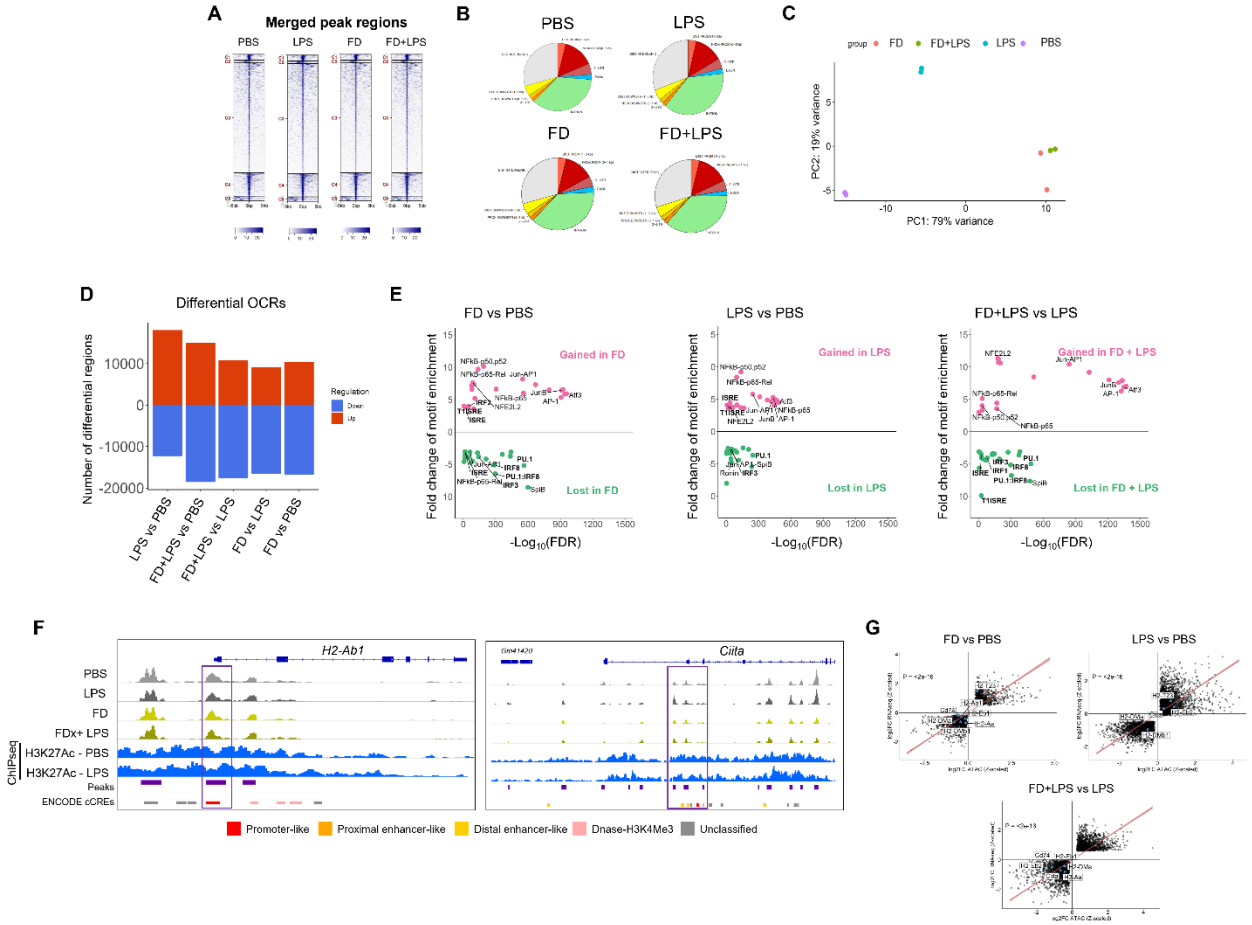

Figure S10. ATAC-seq of BMDCs exposed to FD and LPS. (A) Merged peak regions annotated are shown as an accessibility heatmap. (B) Gene regions of annotated peaks across experimental groups. (C) 2D-PCA plot from DESeq2 normalized OCRs across experimental conditions. (D) Differential number of OCRs analysed via DESeq2. (E) HOMER motif analysis of transcription factors enriched in UP (open chromatin in FD) and DOWN (open chromatin in PBS) peaks. (F) IGV tracks of ATAC-seq BigWig files from each experimental replicate and ChIPseq data from p65 and H3K27Ac in LPS exposed BMDCs, overlayed into mm10 genome. *Ciita* and *H2-Eb1* genes are shown. (G) BMDCs were submitted to ATAC-seq for chromatin accessibility analysis and differential open chromatin regions (OCRs) after pairwise comparison between groups using DESeq2 were integrated with significantly up- or downregulated genes in bulk RNA-seq analysis. A linear regression was traced using z-scaled log2FC from RNA-seq DEGs and ATAC-seq significant ($p<0.05$) differential OCRs.

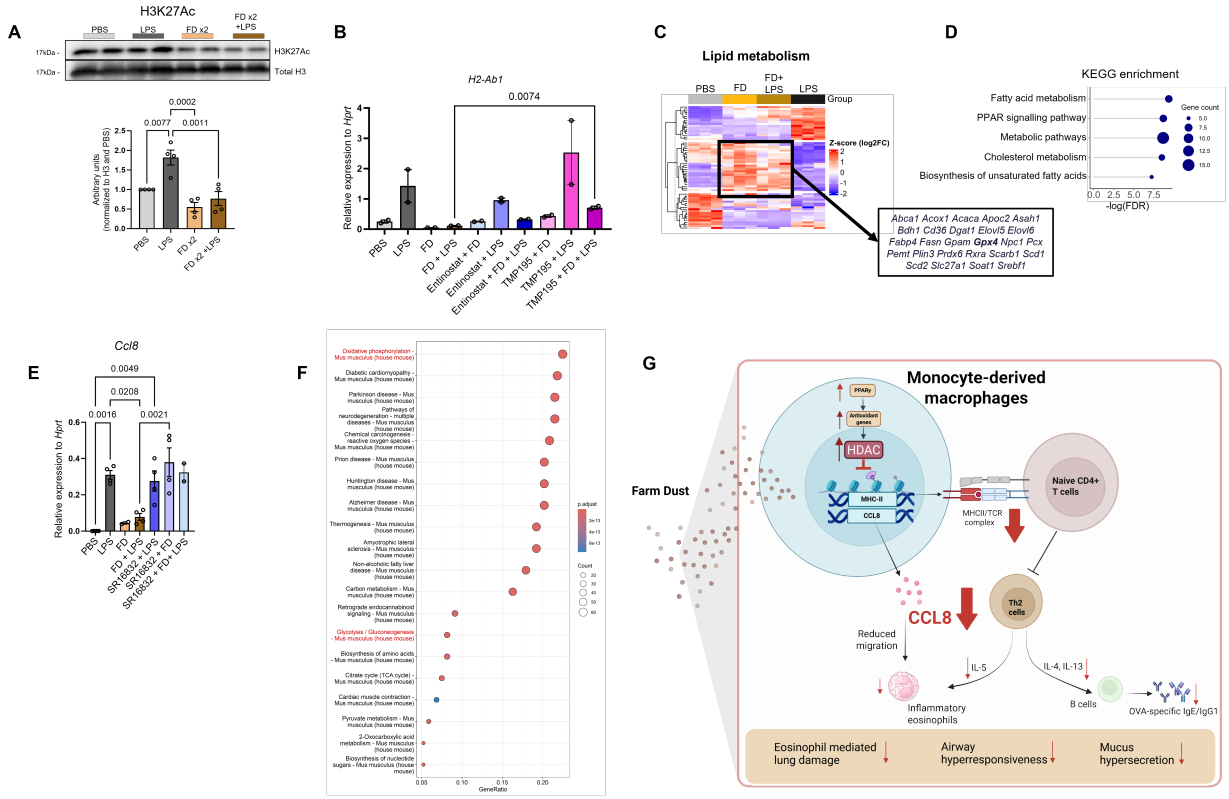

Figure S11. Histone acetylation by HDACs regulates the expression of MHCII genes in BMDMs exposed to FD. (A) The acetylation of the H3K27was measured using Western Blot and normalized to total H3 within nuclear extracts from BMDMs. (B) BMDMs were stimulated with FD for 48h and concomitantly treated with class I HDAC inhibitor entinostat, HDAC3 inhibitor RGFP966 and class IIa HDAC inhibitor TMP195. Next, cells were exposed to LPS for 6h and expression of *H2-Ab1* gene assessed via RT-qPCR. (C) BMDM derived normalized gene counts from genes related to lipid uptake and transport, fatty acid synthesis and oxidation, lipid storage and droplet formation, cholesterol and lipoprotein metabolism and transport, lipid mediated signalling, sphingolipid metabolism and signalling and lipid peroxidation and antioxidant defences were plotted and compared between PBS, PLS, FD and FD+LPS groups. K-means clustering indicated 3 clusters of genes, of which cluster 2 consisted of genes upregulated in FD exposed cells. The genes belonging to this cluster are highlighted. (D) GSEA was performed using this list of genes and associated enriched KEGG pathways were plotted ordered by FDR values. (E) The expression of *Ccl8* was assessed via RT-qPCR in BMDMs exposed to FD, where the dual-allosteric PPARγ inhibitor SR1632 was concomitantly added. (F) Single-cell RNA sequencing (scRNA-seq) analysis comparing MDMs in OVA_FD-treated group and OVA-group, focusing on the KEGG pathways (glycolysis and oxidative phosphorylation combined). (G) Proposed mechanism underlying preventive FD protection from allergic lung inflammation. Results are plotted as mean ±SEM and difference between means were compared using One-way ANOVA followed by Tukey post-hoc test. Difference between FD + LPS and TMP195 + FD + LPS means in panel b was assessed via unpaired Student´s T-test (n=2-6).

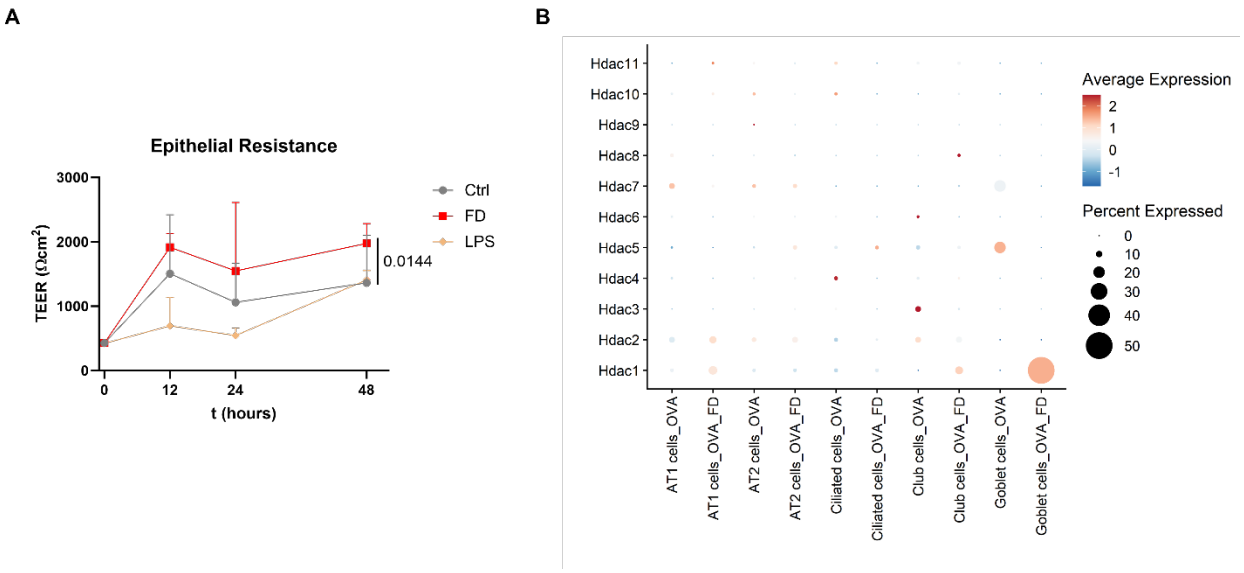

Figure S12. FD enhances epithelial barrier function and alters HDAC gene expression in airway epithelial cells. (A) 16HBE cells were seeded on 0.4 µm transwell inserts and transepithelial electrical resistance (TEER) was measured at 12 h, 24 h, and 48 h following treatment with farm dust. TEER quantifies the electrical resistance across a cellular barrier, reflecting the strength of tight junctions and overall barrier integrity. Compared to controls, farm dust treatment led to a significant increase in TEER values, indicating enhanced epithelial tight junction function and strengthened barrier properties. Results are plotted as mean ±SEM and difference between means were compared using TWO-way ANOVA. The statistically significant difference was observed specifically between the FD-treated group and the LPS-stimulated groups (n=2-4). (B) Average gene expression of selected HDAC genes in major epithelial cell types—Alveolar Type 1 (AT1), Alveolar Type 2 (AT2), Ciliated, Club, and Goblet cells—derived from single-cell RNA sequencing (scRNA-seq) analysis. Expression levels are compared between the OVA control and the OVA+FD-treated groups.

A

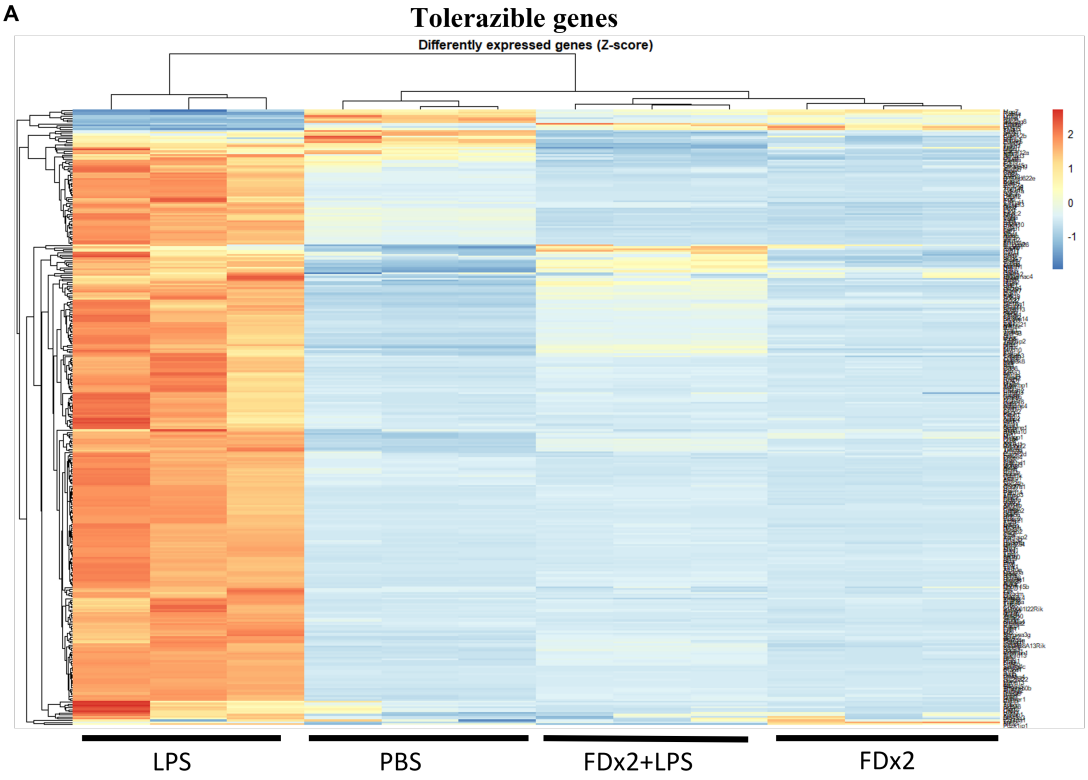
Tolerazible genes
Differently expressed genes (Z-score)
2
1
0
-1
LPS
PBS
FDx2+LPS
FDx2

B

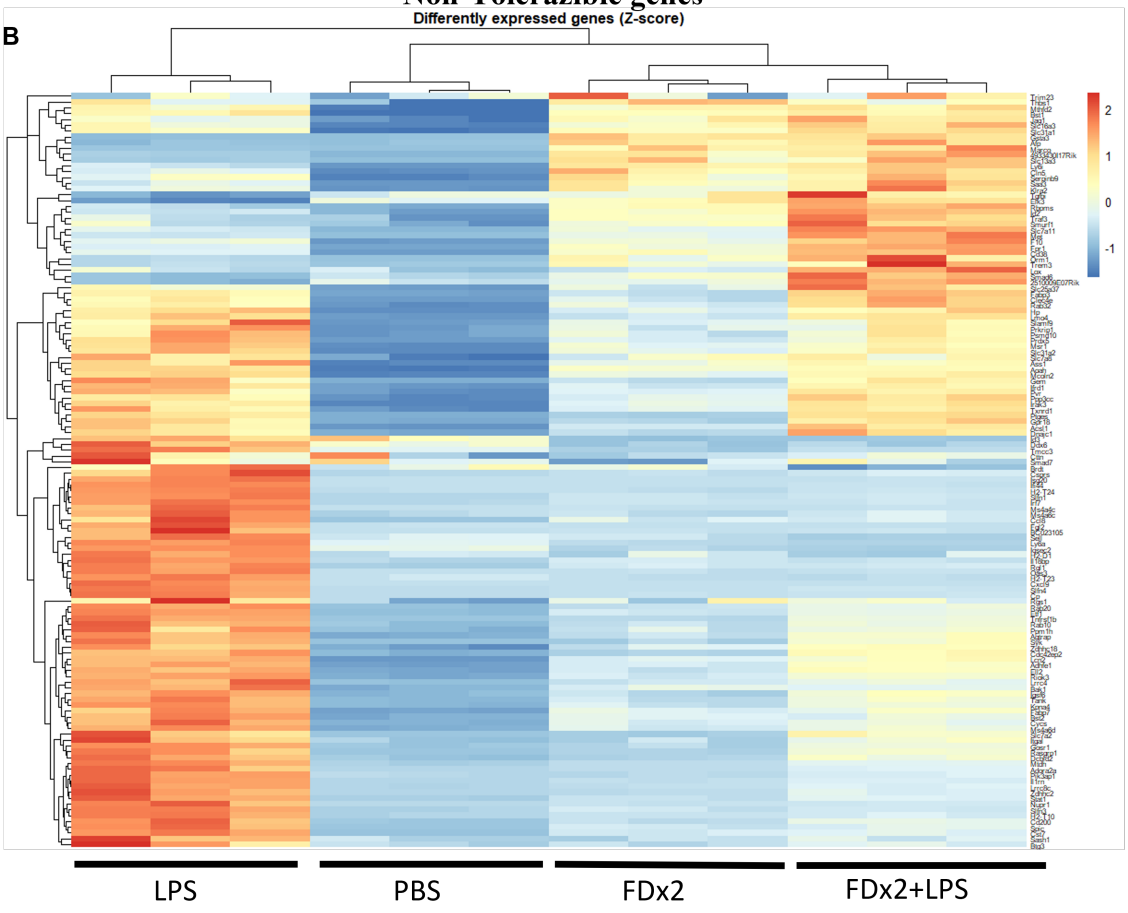
Non-Tolerazible genes
Differently expressed genes (Z-score)
2
1
0
-1
LPS
PBS
FDx2
FDx2+LPS

Figure S13. **FD pretreatment alters LPS-induced gene expression in BMDMs, including unexpected tolerization of non-tolerizeable genes.** RNA sequencing analysis was performed on BMDMs pretreated with FD and subsequently stimulated with LPS. Genes were classified as LPS-tolerized or LPS non-tolerizeable based on the definitions established by Foster et al., 2007 (34). (a) FD treatment suppresses many genes typically tolerized by LPS. (b) FD also suppresses a distinct subset of genes defined as non-tolerizeable.

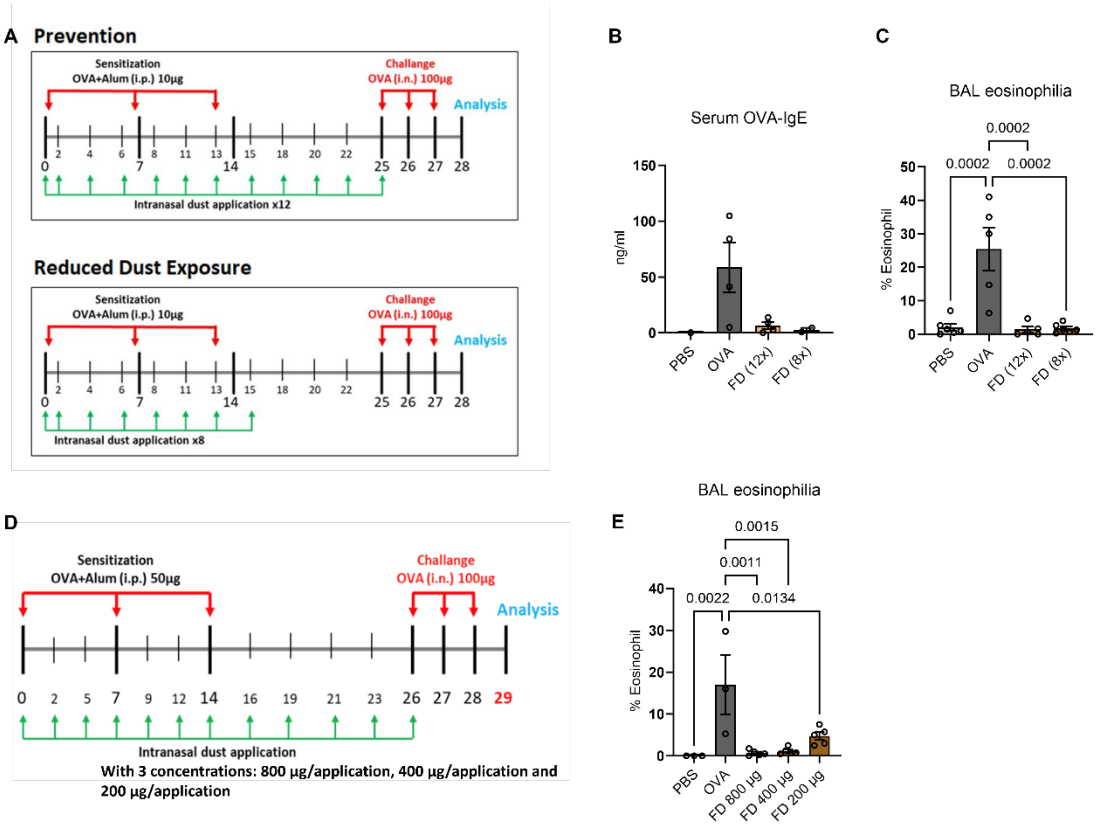

Figure S14. Optimization of dust exposure concentration and timing in the mouse model. (A) Schematic of mouse model exposed to dust 12 times or 8 times. (B) Quantification of eosinophils in BAL fluid. (C) Schematic of mouse model exposed to three different dust concentrations: 800 µg/application, 400 µg/application, and 200 µg/application. (D) Quantification of BAL eosinophilia across concentration groups. Results are plotted as mean ±SEM and difference between means were compared using One-way ANOVA (n=3-6).

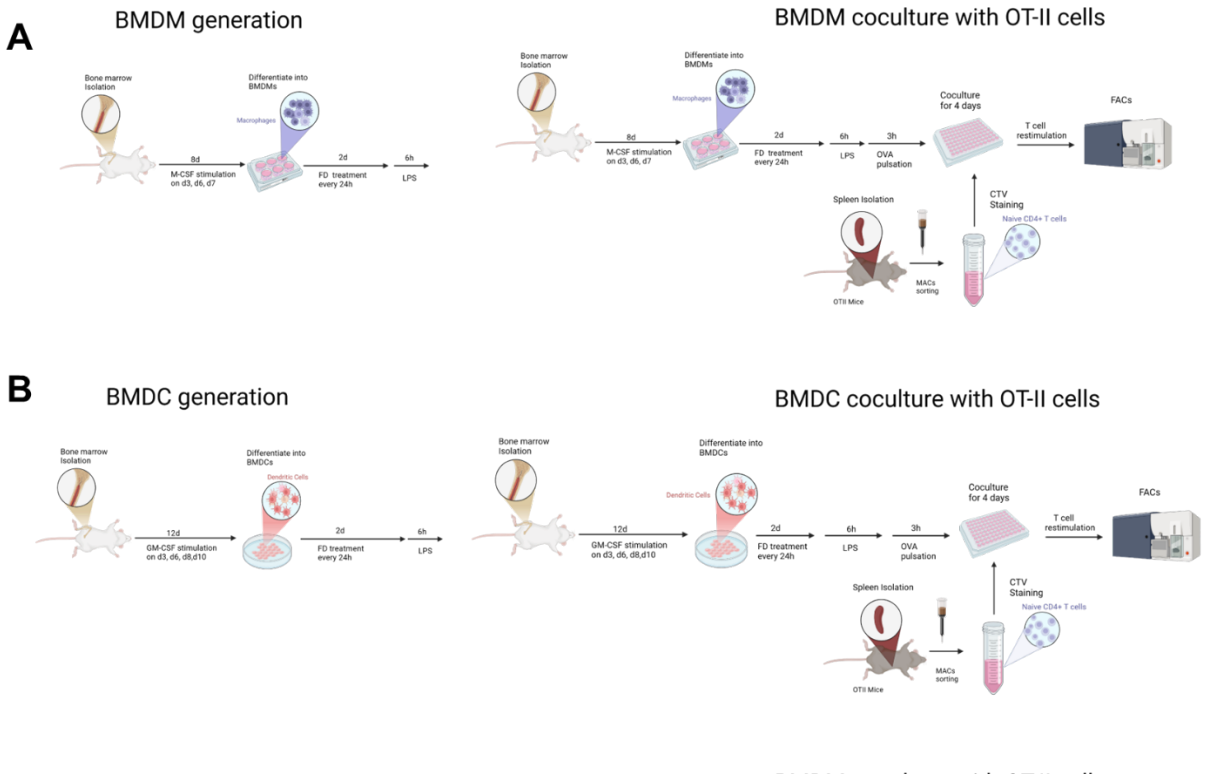

Figure S15. Protocol applied for the generation and co-culture of (A) BMDMs and (B) BMDCs with spleen derived OT-II cells.

Supplemental Data

Antibodies for flow cytometry (clone)	**Company**	**Catalog number**
anti-mouse CD45-BV510 (30-F11)	Biolegend	103138
anti-mouse Siglec-F-BV421 (E50-2440)	BD Biosciences	565934
anti-mouse MHC Class II-FITC (REA813)	Miltenyi Biotec	130112229
anti-mouse FoxP3-PE (REA788)	Miltenyi Biotec	130111600
anti-mouse GATA3-PerCP/Cyanine5.5 (16E10A23)	Miltenyi Biotec	653812
anti-mouse CD4 PE-Vio770 (REA1211)	Miltenyi Biotec	130123211
anti-mouse CD25 BV421 (PC61)	BD Biosciences	562606
anti-mouse T-bet PE/Diazzle (4B10)	Biolegend	644827
anti-mouse Ki67 BV421 (SolA15)	Invitrogen	404569892
anti-mouse CCR2-BV650 (SA203G11)	Biolegend	150613
anti-mouse CD11b-FITC (REA592)	Miltenyi Biotec	130113811
anti-mouse CD11c-APC (REA754)	Miltenyi Biotec	130110702
anti-mouse F4/80-PE-Cy7 (REA126)	Miltenyi Biotec	130118459
anti-mouse CD19-APC (REA749)	Miltenyi Biotec	130112036
anti-mouse CD45-PE-cy7 (REA737)	Miltenyi Biotec	130110799
anti-mouse CD3-APC-cy7 (REA641)	Miltenyi Biotec	130119793
anti-mouse CD206-BV785 (C068C2)	Miltenyi Biotec	141729
anti- mouse CD86-APC (PO3)	Biolegend	105113
anti-mouse CD80-APC-cy7 (REA9831)	Miltenyi Biotec	130116463
anti-mouse CD45-APC-cy7 (30-F11)	BD Biosciences	557659
anti-mouse CD11c-BV711(N418)	Miltenyi Biotec	117349
anti-mouse CD11b-APC-cy7(M1/70)	Invitrogen	B2721-NI43U
anti-mouse CD80-PE(16-10A1)	Miltenyi Biotec	130102613
anti-mouse CD62L-APC(MEL-14)	Invitrogen	17062182
anti-mouse CD16/CD32(93)	Invitrogen	2334894
anti-mouse CD64-BV711 (X54-5/7.1)	Miltenyi Biotec	139311
anti-mouse CD103-PerCP-5.5 (2E7)	Biolegend	121416
anti-mouse CD19-Pacific blue(1D3)	BD Biosciences	560375
anti-mouse CD3-Pacific blue(17A2)	Invitrogen	2619654
anti-mouse CD49b-Pacific blue(DX5)	Biolegend	108918
anti-mouse Ly6G-Pacific blue(1A8)	Biolegend	127612
anti-Human HLA-DR PerCP-Cy5.5 (G46-6)	BD Biosciences	560652
Antibodies for *in vivo* administration (clone)	**Company**	**Catalog number**
Purified Rat IgG2b, κ Isotype Ctrl Antibody (RTK4530)	BioLegend	400601
anti-mouse CCL8 (A16070K)	BioLegend	536902
Antibodies for western blot (clone)	**Company**	**Catalog number**
anti-acetyl-Histone H3 (Lys27) (D5E4)	Cell Signalling Technology	#8173
anti- Histone H3 (D1H2)	Cell Signalling Technology	#4499
Antibodies for IHC or IF (clone)	**Company**	**Catalog number**
Anti-CD11b antibody (EPR1344)	Abcam	ab33357
anti-CD68 antibody polyclonal	Abcam	ab125212

Anti-CD11c antibody (EPR21826)	Abcam	ab219799
Anti-ki67 antibody polyclonal	Invitrogen	PA5-19462
Anti-CD4 antibody (EPR19514)	Abcam	ab183685

Table S1. Antibodies used in the study.

Gene	Forward	Reverse
mouse Hprt	CCTAAGATGAGCGCAAGTTGAA	CCACAGGACTAGAACAACTGCTAA
mouse Ccl8	GAAGGGGGATCTTCAGCTTT	TCTTTGCCTGCTGCTCATAG
mouse H2-Ab1	GCGGAGAGTTGAGCCTACG	AGGCCCGTGGACACAATT
mouse Il4	CCCCAGCTAGTTGTCATCCTG	CAAGTGATTTTTGTCGCATCCG
mouse Il5	GCAATGAGACGATGAGGCTTC	GCCCCTGAAAGATTTCTCCAATG
mouse Il13	TAC GGT CTC CAG CCT CCC CG	GGC CGT GGC GAA ACA GTT GC
mouse Il33	TCCTTGCTTGGCAGTATC	TGCTCAATGTGTCAACAGACG
mouse Muc5ac	ATCGAGAGGAGCGTTGACAC	ATGCAGCCTTGCTTGAGG
mouse Gob5	TCTTCCTCTTGATCCTCCACC	GCCCTCATAGCCGTTGTTGT
mouse Spdef	ACGGATGGTGAGGTGGACT	CACCTGTGCTGAGTCCTCAAT
human CCL8	TGGAGAGCTACACAAGAATCACC	TGGTCCAGATGCTTCATGGAA
human HPRT	AGGAAAGCAAAGTCTGCATTGTT	GGTGGAGATGATCTCTCAACTTTAA

Table S2. Primers used for RT-qPCR.

Compound	Catalog number	Concentration	Supplier
RGFP966	HY-13909	1uM	MedChemExpress
Entinostat	HY-12163	1uM	MedChemExpress
TMP195	HY-18361	1uM	MedChemExpress
GW9662	HY-16578	1uM	MedChemExpress
Vorisnostat	HY-10221	1uM	MedChemExpress
Resatorvid	HY-11109	10uM	MedChemExpress
T-5224	HY-12270	10uM	MedChemExpress
ML385	HY-100523	5uM	MedChemExpress
Rosiglitazone	HY-17386	1uM	MedChemExpress
SR 16832	HY-112247	1uM	MedChemExpress
AS1517499	HY-100614	1uM	MedChemExpress
Stattic	HY-13818	10uM	MedChemExpress
IRAK-1-4 Inhibitor I	HY-13329	10uM	MedChemExpress
RSL-3	19288	1uM	Cayman Chemical Company
Thermo Scientific™ Imject™ Alum	77161		Thermo Fisher Scientific
OVA grade VI	A2512		Sigma Aldrich
OVA grade V	A5503		Sigma Aldrich
Ovalbumin (323-339)	O164		Sigma Aldrich
Lipopolysaccharides from Escherichia coli O55:B5	L2880		Sigma Aldrich
Recombinant mGM-CSF	#12343127		ImmunoTools
Recombinant mM-CSF	#12343137		ImmunoTools
Recombinant hGM-CSF	#11343125		ImmunoTools

Table S3. Compounds and concentrations used in the study.